REPRINT: accepted manuscript with proof, NF 2020, DOI 10.1088/1741-4326/abd63f

The evolution of the bound particle reservoir in Wendelstein 7-X and its influence on plasma control

G. Schlisio,[1,*] U. Wenzel,[1] D. Naujoks,[1] T.S. Pedersen,[1] H. Grote,[1] V.R. Winters,[1] H. Niemann,[1] M. Mulsow,[1] M. Krychowiak,[1] P. Drewelow,[1] Y. Gao,[1] M. Jakubowski,[1] A. Puig Sitjes,[1] H. Laqua,[1] J. Knauer,[1] K.J. Brunner,[1] and the W7-X team[b]

[1] *Max-Planck-Institut für Plasmaphysik, Wendelsteinstraße 1, 17491 Greifswald, Germany*

(Dated: January 6, 2021)

Abstract

The investigation of fuel retention in fusion experiments is important in view of plasma density control as well as tritium inventory for future fusion reactors. We present a first gas balance of the stellarator Wendelstein 7-X with its inertially cooled graphite divertor. The gas balance is used to estimate the wall inventory and it is found that the wall plays an important and dynamic role, absorbing or releasing particles depending on the plasma conditions. Several different scenarios are presented and the effect of fueling and heating on the wall inventory is assessed. We find that the record duration plasma experiment of 100 s required previous shorter plasmas to be successfully conducted.

[b] See author list of T. Klinger et al., Nuclear Fusion 59 (2019) 112004

[*] georg.schlisio@ipp.mpg.de

I. INTRODUCTION

Future fusion reactors face a number of yet unsolved problems, such as power and particle exhaust, both related to the boundary of the plasma. The interaction between energetic plasma particles and the wall leads to particles being retained and released on the walls. This results in a coupling of plasma and wall in terms of particles, which in turn influences core particle content and has the potential to degrade density control. For reactor-like steady-state fusion plasmas, e.g. ITER, this has to be solved by a net-zero particle flux between plasma and surrounding wall [1].

Wendelstein 7-X (W7-X) is an optimized modular stellarator [2] designed for steady-state operation with parameters approaching those of a reactor for up to 30 min of continuous plasma and as such a promising test bed for these problems. W7-X is outfitted with carbon tiles on the heat shields and divertors and cooled stainless steel panels in low loaded areas [3]. All these plasma facing surfaces will be referred to as *first wall* in this treatment.

W7-X was in first commissioning operation (OP1.1) in 2015 with a graphite limiter [4]. In its second operation phase, OP1.2 in 2017 and 2018, it was operated with an inertially cooled graphite divertor and an extended set of diagnostics [5]. Currently 10 water-cooled carbon-fiber-composite (CFC) divertors are being installed and will be commissioned and operated in the next campaigns, here collectively referred to as operation phase 2 (OP2). The island divertor in W7-X is toroidally varying and segmented, intersecting magnetic islands in each module.

In this paper we present an analysis of the evolution of the wall particle reservoir of W7-X as found with the inertially cooled divertor in OP1.2 in attached plasmas. The wall reservoir is obtained from a gas balance as a balance of injected and removed particles.

Gas balances have been calculated for most major fusion experiments, such as DIII-D [6], ASDEX Upgrade [7, 8], LHD [9, 10], JET [11] and KSTAR [12]. Significant hydrogen retention is commonly found in carbon machines [13] and frequently attributed to amorphous carbon layers (so-called a:CH layers) [14] as well as implantation, but net outgassing scenarios are found as well.

Section II introduces the basic concepts and methodology and deals with the assumptions necessary. In section III a simple W7-X plasma is introduced and the results are discussed. In section IV a sequence of two plasmas and the influence of plasma conditions are investigated. Section V explains the gas balance of the way to the record duration plasma in OP1.2b.

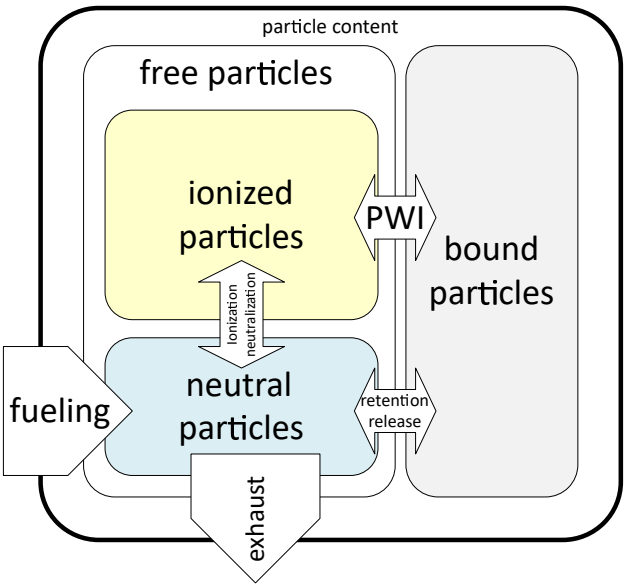

FIG. 1. Schematic view of the reservoir model. The outer contour symbolizes the plasma vessel, subdivision of the particle content according to equation (1). Arrows indicate migration between reservoirs and are annotated with the main mechanisms. The role of NBI is left out for simplicity. (color online)

II. CONCEPTS, METHODOLOGY, AND ASSUMPTIONS

In a reactor inventory accounting will be of high importance when regulatory rules require a close monitoring of radioactive material, especially tritium. Common fusion experiments are not well equipped for detailed accounting and balancing, but existing diagnostics can be used to augment a 0D model. The assumption of a simple continuity equation balancing cumulated injection rate $\int \dot{N}_{in}$ and exhaust rate $\int \dot{N}_{out}$ assumes no particles being generated or lost inside the experiment and is a good first-order approximation. The particle content can now be split up into different reservoirs: free neutral particles N_n, plasma molecular equivalent N_p and bound particles N_w bound in the wall. A visual representation is given in figure 1. All reservoirs except the bound reservoir start at zero or close to zero at the beginning of a plasma pulse, and since analysis is done pulse by pulse, we introduce an offset $N_{w,0}$ representing the unknown wall content at heating start.

$$\int_{t_0}^{t} \dot{N}_{in} - \int_{t_0}^{t} \dot{N}_{out} = N_n + N_p + N_w - N_{w,0} \tag{1}$$

Particles are counted in units of their chemically stable state, e.g. molecules. In W7-X the main gas species is hydrogen, while especially in the beginning of the campaign helium was used for conditioning. All investigated experiments in this study were conducted with hydrogen.

The assumption of a continuity equation as stable particles with no chemical change has to be relaxed for plasma chemistry as well as fuel burnup and He-ash formation in a reactor. That leads to a coupling term between the balances for different species. One example is the carbon chemistry on the large carbon surface of the first wall, carbohydrates as well as carbon oxides can be regularly observed in the exhaust gas in small quantities, e.g. by means of a residual gas analyser (RGA) [15]. With increasing tungsten surface [16] and continued nitrogen seeding [17] ammonia formation [18] could become a noticeable phenomenon in W7-X as well. This is neglected here, since it does not play a role in W7-X at least for hydrogen as majority plasma species investigated here.

Not all of the parameters in equation (1) are easily accessible and for some only rough estimates exist. This requires making some assumptions or estimations, discussed below.

A. Plasma molecular equivalent N_p

The estimation of plasma molecular equivalent is retrieved from the line integrated density measurement and geometric factors for hydrogen as

$$N_p = \frac{1}{2}\frac{n_e V_p}{l} \cdot \left(1 - \sum_i f_i \cdot Z_i\right) \tag{2}$$

with the line-integrated density n_e, the sight line length l, the plasma volume V_p and the impurity fraction f_i and atomic number Z_i. The line-integrated density is measured with an interferometer [19] with a sight line of 1.33 m in plasma. This length varies with magnetic configuration and plasma beta below 4 % and is assumed constant.

The factor $(1 - \sum_i f_i \cdot Z_i)$ corrects the electron density for the additional electrons from impurities to obtain the number of hydrogen ions. Assuming an example case of an impurity fraction f_i of 2 % carbon and 1 % oxygen in hydrogen, neglecting further possible impurities and assuming complete ionization of all impurities yields a correction factor of 0.8. This scenario is an upper estimate for W7-X OP1.2b post boronization, and the effect on the following analysis is small, so we assume this to be constant at the stated levels. Impurity content is W7-X is monitored with a number of diagnostics, such as charge exchange recombination spectroscopy [20], soft-x-ray pulse height analysis [21], ultraviolet overview spectroscopy [22] and Z_{eff} diagnostic [23].

The plasma volume V_p of W7-X is about 28 m^3 and changes only little in the type of experiment investigated here. We assume that only a negligible amount of ionized particles exists outside of

this volume. Since we account for molecules in all other reservoirs, the obtained atom number has to be converted to molecules by dividing by the number of atoms per molecule, which is 2 for hydrogen.

B. Neutral particle content N_n

Neutral particle content N_n is determined by pressure measurement, the ideal gas law, and temperature and geometric assumptions:

$$N_n = \frac{pV_n}{k_B T} \tag{3}$$

with the pressure p, the neutral volume V_n, the Boltzmann constant k_B and the gas temperature T.

The total plasma vessel volume is about $110\,\mathrm{m}^3$, but does not always represent the neutral volume. During plasma operation, it is reduced by the plasma volume, where due to high plasma temperatures and densities neutrals are ionized within short distance of flight. This is confirmed by H_α emission indicating ionization only in a thin boundary layer.

W7-X utilizes hot cathode ionization gauges suited for long-pulse operation [24], based on ASDEX gauges common in tokamaks [25], to measure in-vessel pressure with high time resolution. These are supplemented with a set of in-situ Penning gauges [26] and low-sampled commercial Penning gauges for operational and long-term monitoring of vacuum conditions [27].

Due to the overall availability of measurements in quantities of volume times pressure (per unit time for fluxes), the ideal gas law is used to convert measurements to absolute particle numbers. While the ideal gas law is suitable for most gases at low pressures and temperatures far away from phase boundaries, the neutral momentum distribution does not necessarily always follow a Maxwellian distribution required for the definition of a temperature. Nonetheless, lacking a practical alternative, and for reasons of simplicity, a Maxwellian distribution is assumed in this study.

The neutral temperature depends on the position of measurement and the plasma conditions, but is assumed to be constant over the whole evaluation domain at a value of 300 K unless stated otherwise. This is the cooling water temperature of the plasma vessel and thus the equilibrium temperature for gas after several collisions with the wall structure.

The validity of this assumption is confirmed by EMC3-EIRENE [28] simulations shown in figure 2 and can be explained by molecules forming on the wall and thus being thermalized there.

In the simulations, atoms show a much higher temperature, which is understood as that they most likely originate from charge exchange and dissociation processes closer to the plasma. Due to their low absolute numbers they do not significantly contribute to the neutral pressure and can be neglected here.

During plasma operation, the pressure value inside and outside the divertor differ significantly. This is desired, as it greatly enhances particle exhaust while keeping the neutral influx into the main plasma low. On the other hand it requires to split the neutral volume into smaller parts, to get a more fine-grained estimation of neutral particle content. The sub-divertor space in OP1.2 was estimated from CAD with $5.12\,\mathrm{m}^3$ for the low-iota part and $0.47\,\mathrm{m}^3$ for the high-iota part, two segments of the divertor named for the configurations in which they are used. Their sub-divertor volumes are separated by closures and pumped through different ports. Pressure in the low-iota sub-divertor space is averaged between the measurement locations in the pumping port and in the pumping gap, in the high-iota part measured in the pumping port, and in the main chamber in the outer midplane. See figure 3 for a sketch of the gauge positions.

C. Removed particles

Pump performance is given as *pumping speed S* in units of volume per unit time. The exhaust rate Q is then given by the product of pumping speed S and pressure p, but again conversion to absolute particle numbers with the ideal gas law requires a gas temperature T:

$$Q = p \cdot S, \tag{4}$$

$$\dot{N}_{out} = \frac{Q}{k_B T}. \tag{5}$$

Since the main pumps at W7-X are located in receded positions due to low magnetic field acceptance, particles thermalize on the duct walls and can safely be assumed to have reached vessel temperature when being pumped.

In OP1, W7-X's main pumping system consists of 30 turbo-molecular pumps (TMPs) with a total pumping speed of $30\,\mathrm{m}^3/\mathrm{s}$ in hydrogen during OP1.2. With the new water-cooled divertor installed for OP2, pumping is enhanced by additional cryopumps with an approximate pumping speed of $75\,\mathrm{m}^3/\mathrm{s}$. With pressures below $1 \cdot 10^{-3}$ mbar at the pump inlet, the pumping speed does not depend on the pressure and the exhaust rate is only determined by the inlet pressure.

Various diagnostic pumps exist, but contribute only negligible pumping speed and are often

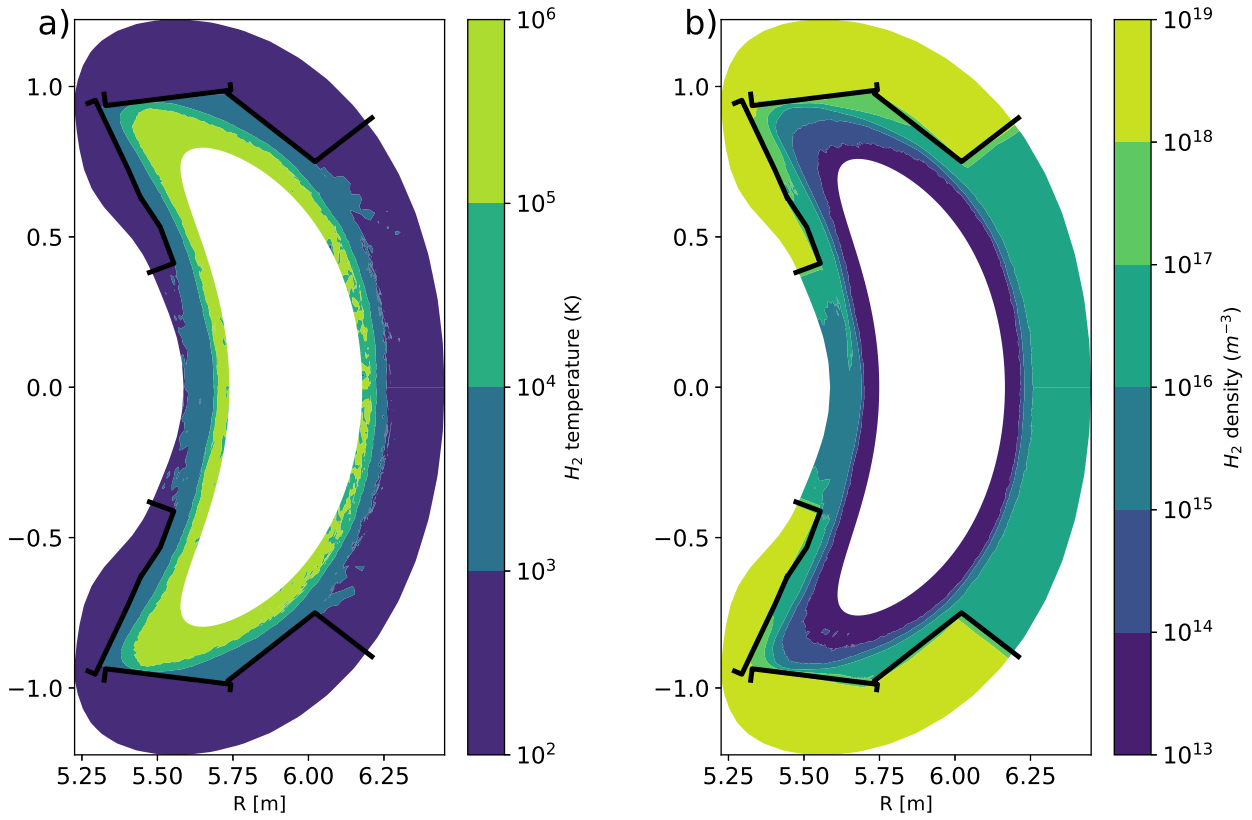

FIG. 2. Simulation of neutral gas properties in the bean-shaped cross-section of W7-X ($\phi = 0$) from EMC3-EIRENE, overplottet with first wall structures in black. Simulated plasma parameters: $P_{ECRH} = 4.5\,\mathrm{MW}$, $D = 1\,\mathrm{m^2\,s^{-1}}$, $\chi = 3 \cdot D$, $n_{e,s} = 1 \cdot 10^{19}\,\mathrm{m^{-3}}$, EIM magnetic configuration without error field correction. **a)**: Temperature. Cold neutrals outside the plasma are visible, core domain excluded. **b)**: H_2 molecular density. Distinct reservoirs are visible: *Inside the plasma*, only negligible particle densities are found, *surrounding the plasma* is a region of medium pressure and the *subdivertor* space shows much higher densities. This simulation is not intended for quantitative use, but meant to illustrate and motivate the different reservoirs. Molecule density was capped at $10 \cdot 10^{13}\,\mathrm{m^{-3}}$ excluding the noisy plasma core. The subdivertor geometry is not reproduced properly here, so no inference on subdivertor volume is possible from this plot. (color online)

mounted in low-conductivity ducts further reducing the pump rate. They are not considered in this work.

Pumping of the NBI box is achieved by titanium getter pumps, which have a very high initial

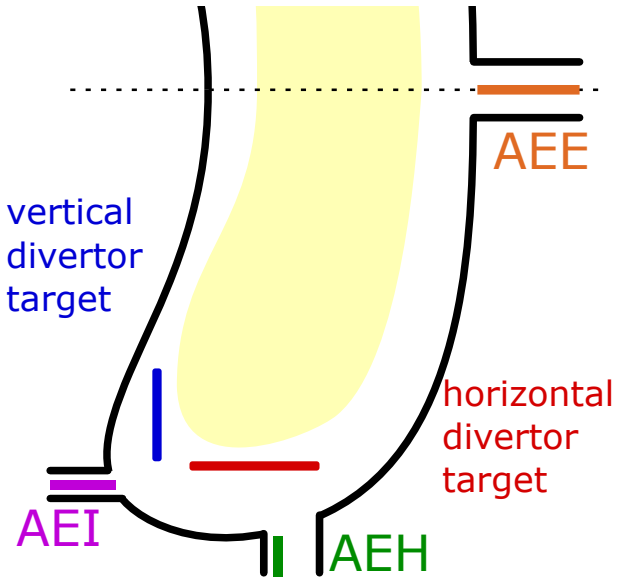

FIG. 3. Schematic poloidal cut of W7-X to illustrate the total pressure gauge position. The plasma vessel shown in black, divertor target plates in blue (vertical) and red (horizontal), relevant measurement locations: AEE - outer midplane, AEH - pumping port, AEI - pumping gap. Central yellow shade symbolizes plasma region. Additional in-vessel components, such as baffles and heat shields, are not shown. The term *pumping gap* refers to the gap between horizontal and vertical divertor target, where neutral particles enter the sub-divertor space. The divertor has a segment used in *high iota* magnetic configuration, located in a toroidally shifted location. There, only a horizontal target and a pumping port measurement location exists. Adapted from [24]. (color online)

pumping speed degrading over time. The NBI box in connected to the W7-X plasma vessel with a large duct typically closed by a gate valve. The exact amount of pumped particles due to NBI operation is not known, because relevant gauges malfunctioned during operation. NBI experiments were excluded from this work, with one exception. Implications on the exception are discussed in section V.

D. Injected particles

The particle sources comprise all external particle sources, such as gas valves, pellet injectors, diagnostic and heating particle beams as well as leaks. In W7-X there is a main fueling valve system [29], a divertor gas inlet system [30], a frozen pellet injector [31] [32], an impurity pellet

injector [33], an impurity laser sputtering device [34] and a neutral beam injection (NBI) system [35] as particle sources.

Only the main valve system, the divertor gas inlet, frozen pellet injector and NBI significantly contribute to the particle inventory and for simplicity reasons, only experiments utilizing the main fueling valves were selected for this investigation.

The valve system use piezo valves augmented with a Pirani flow sensor with an output in pressure times volume per unit time. They were calibrated for each gas with injections into the evacuated vessel. For the injected gas, vessel temperature is assumed. Their calibration was conducted in cold state and measured temperature of the fueling gas reservoirs were not significantly different from cooling water temperature.

E. bound particles

The bound particle reservoir is only indirectly quantifiable and is expected to be the largest. Depending on material properties and first-wall treatment, e.g. by wall conditioning, vacuum conditions, plasma wetting and heating, this reservoir can change significantly from discharge to discharge.

Unless the other reservoirs, its initial value is neither zero nor easily known, and consists of retained particles in the first wall material that can be mobilized under certain conditions. Graphite, the main material for plasma facing components in W7-X, is known to absorb large amounts of water. After boronization, oxygen is efficiently captured and water is released as hydrogen only. All scenarios discussed were conducted after boronization.

III. BASIC PLASMA

A typical simple plasma in W7-X during OP1.2 was heated by pure electron cyclotron heating (ECRH), prefilled with a hydrogen gas puff of $3 \cdot 10^{20}$ molecules and continuously fueled from a mid-plane position via feedback control on a constant pre-set value of the line integrated density signal. More complex experiments were conducted, including frozen hydrogen pellet injection, impurity injection, NBI diagnostic and heating operation, density ramps and more, but are not addressed in this study for simplicity.

Figure 4 shows the gas balance of an example plasma of the W7-X inertially cooled divertor

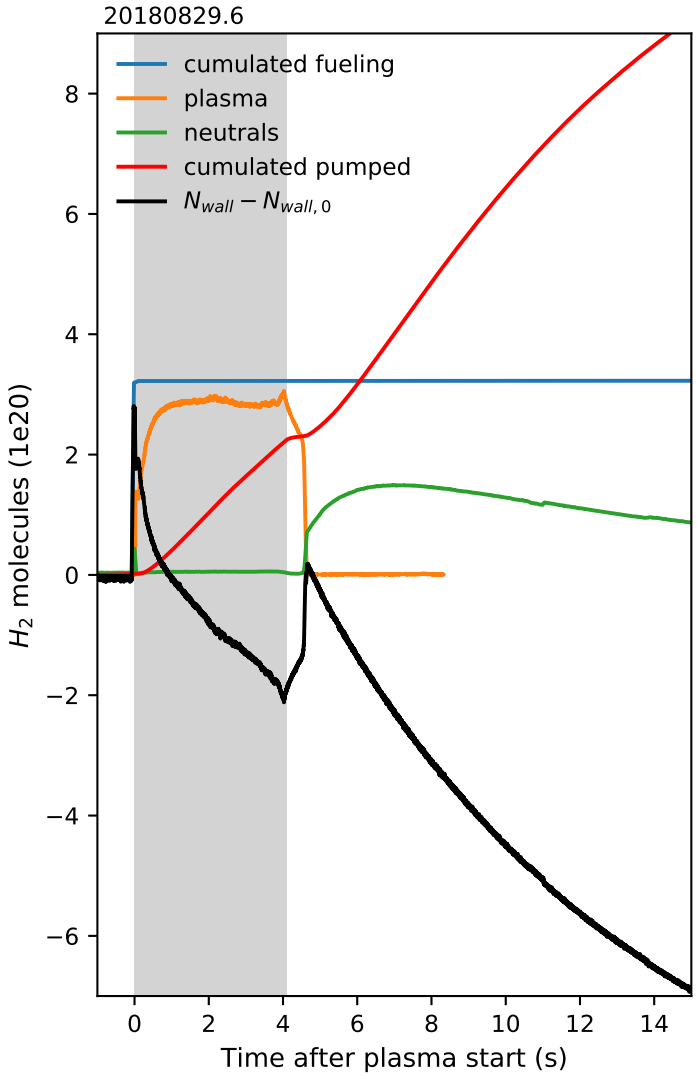

FIG. 4. Gas balance of a basic exemplary plasma of OP1.2 with inertially cooled divertor after boronization. Cumulated fueling (blue) and exhaust (red) are shown along with the plasma molecular equivalent(orange) and the total neutral inventory (green). Net wall content (black) derived according to equation (1). Plasma heating phase with pure ECRH is indicated with grey shade. (color online)

campaign (OP1.2) after boronization, conducted in the so-called *low iota* magnetic configuration. It is heated with 4 MW ECRH, fueled with hydrogen gas and reaches a line-integrated density of $3.5 \cdot 10^{19}\,\mathrm{m}^{-2}$ line integrated electron density which amounts to ca. $2.5 \cdot 10^{20}$ molecules. The target line-integrated density of $2 \cdot 10^{19}\,\mathrm{m}^{-2}$ was continuously exceeded, so no additional fueling was applied during the whole duration of the 4 second program.

The plasma reservoir is fed by most of the gas prefill and quickly attaches to the wall, where the hot plasma forms a barrier for neutral particles from the strikeline (divertor plugging [36]). This results in a rise of the sub-divertor pressure and significant particle exhaust according to equation (5). By the end of heating, about as much gas was exhausted as was ionized, with the wall releasing a significant amount of particles as well.

At the end of heating the plasma quickly disappears and the recombinating particles form a

significant neutral reservoir, which is however not as large as the plasma reservoir. Most of the particles remain in the wall, but start outgassing over a longer timespan. The lowest sub-divertor pressure is found at the beginning and end of plasma, when the plasma is not attached to the divertor target plates and neutrals are not efficiently compressed into the pumping gap. Within seconds after plasma decay, the outgassing fills the plasma vessel and allows efficient particle exhaust again.

The shown example yield a net outgassing of the wall of about $2 \cdot 10^{20}$ particles by the end of heating but mobilized a much greater reservoir for the subsequent outgassing phase. With a total net outgassing of about $2.3 \cdot 10^{21}$ particles this plasma can be classified as having a wall conditioning effect, removing about eight times as much as fueled.

Comparison of typical particle reservoir sizes

For illustration purpose, typical reservoir sizes at relevant parameters are given in table I. One clearly sees that the neutral reservoirs during and before plasma do usually not contribute significantly to the plasma vessel particle content, either due to their small size in the case of the sub-divertor space or due to the low pressure. Only during the outgassing phase following successful divertor target heating, the neutral reservoir transiently becomes a major contribution in the balance.

The derived numbers partially match with the modelling from [27]. Good agreement is found in the fueling rate, and also for the exhaust rate, as a sub-divertor pressure of $1 \cdot 10^{-3}$ mbar was assumed in that study.

Estimating the wall particle reservoir can only be done with rough estimations due to many unknowns.

Literature treatments distinguish between surface and bulk retention. The surface reservoir is given with $10^{18}\,\mathrm{cm}^{-2}$ [37] in graphite, which amounts to about $2 \cdot 10^{23}$ particles on the divertor ($20\,\mathrm{m}^2$) and $1 \cdot 10^{24}$ particles for the total $105\,\mathrm{m}^2$ of carbon surfaces in W7-X.

With the primary interaction surface on the divertor of a about $1\,\mathrm{m}^2$ [38] (up to $1.5\,\mathrm{m}^2$, but only about $0.5\,\mathrm{m}^2$ in *high iota* configuration), $1 \cdot 10^{22}$ particles in the surface area are directly accessible to the plasma.

Bulk retention in the divertor tiles with a thickness of 3 cm (graphite volume of about $0.6\,\mathrm{m}^3$ and a weight of about 1076 kg) can be estimated to about $1.6 \cdot 10^{24}$ particles (5 g/t [39]) of hydrogen.

Reservoir description	**typical size or rate (molecules)**
prefill	$3 \cdot 10^{20}$
maximum fueling from one valve[a]	$1.7 \cdot 10^{21}\,\mathrm{s}^{-1}$
plasma particle content (at $1 \cdot 10^{20}$ electrons$/\mathrm{m}^2$)	$9 \cdot 10^{20}$
neutral background pre-operation (at $1 \cdot 10^{-7}$ mbar)	$2 \cdot 10^{17}$
midplane neutral reservoir during plasma (at $3 \cdot 10^{-6}$ mbar)	$6.2 \cdot 10^{18}$
divertor neutral reservoir during plasma (at $1 \cdot 10^{-4}$ mbar)	$1.2 \cdot 10^{19}$
neutral reservoir during outgassing phase (at $1 \cdot 10^{-4}$ mbar)	$2.7 \cdot 10^{20}$
pumped H_2 OP1.2 (TMP only: $30\,\mathrm{m}^3/\mathrm{s}$) (at $1 \cdot 10^{-4}$ mbar)	$7 \cdot 10^{19}\,\mathrm{s}^{-1}$
projected pumping H_2 OP2 (TMP + cryo pump: $105\,\mathrm{m}^3/\mathrm{s}$) (at $1 \cdot 10^{-4}$ mbar)	$2.5 \cdot 10^{20}\,\mathrm{s}^{-1}$
H_2 surface and bulk retention in the carbon divertor [b]	$1.8 \cdot 10^{24}$
H_2 surface retention in the strike line [c]	$1 \cdot 10^{22}$
H_2 surface retention in steel	$7 \cdot 10^{23}$

[a] main gas valve system, 11 valves in total, individual values vary up to $\pm 30\%$

[b] estimate, see text for details

[c] see text for details

TABLE I. Comparison of typical reservoir sizes and particle rates. Free neutral inventory only reaches significant size during outgassing, (potential) bound reservoir exceeds all other by far. All conversions assumed at T = 300 K for molecular hydrogen.

This value strongly depends on sample properties [40] but may serve as a rough estimate here.

Other carbon surfaces as the baffles ($35\,\mathrm{m}^2$) and heat shield ($50\,\mathrm{m}^2$) are not designed for direct plasma contact, but may receive varying loads mobilizing retained particles. These effects are neglected here for simplicity reasons.

The hydrogen surface retention in steel is about two orders of magnitude lower than in graphite ($10^{16}\,\mathrm{cm}^{-2}$) [41, 42], and thus yields about $7 \cdot 10^{23}$ particles for the $70\,\mathrm{m}^2$ of steel first wall. Since no steel components are in direct contact with plasma, the bulk retention was not considered relevant.

Further steel surfaces are covered with carbon tiles or extend into the ports, but are not taken

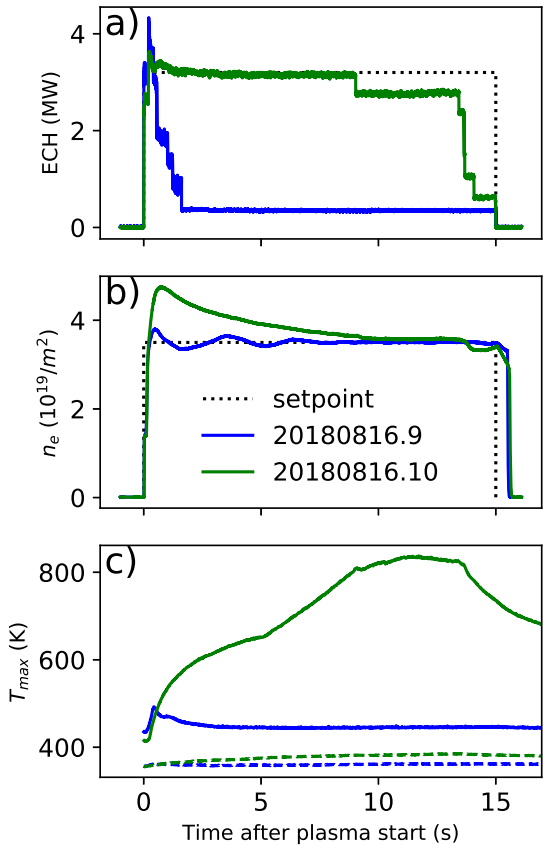

FIG. 5. Comparison of two programs of similar density: panel a: Total heating power, panel b: line-integrated density, panel c: maximum divertor surface temperature (solid line) and baffle temperature (dashed line). Target density and heating power in black, 20180816.9 in blue, 20180816.10 in green. Despite great difference in heating power and deposited energy, the same density is reached. (color online)

into account in this estimation.

In conclusion, the bound reservoirs potentially exceed the other reservoirs by orders of magnitude.

IV. SHORT TERM WALL RESERVOIR

In this section, we will discuss the influence of short-term reservoirs which influence wall behavior of consecutive plasma experiments. The chosen examples were conducted in magnetic standard configuration, and had a programmed duration of 15 s, a target plasma line-integrated density of $3.5 \cdot 10^{19}\,\mathrm{m}^{-2}$ controlled by the fueling system and a nominal heating power of 3.2 MW ECRH. Due to gyrotron issues, the full heating power was not always applied, leading to notable effects on the gas balance.

Of the repetitions, two are of interest: one (20180816.9) ran for the full programmed duration at very low input power of 600 kW and reached target density only with very strong fueling. The following program (20180816.10) was heated with the foreseen heating power and did not require

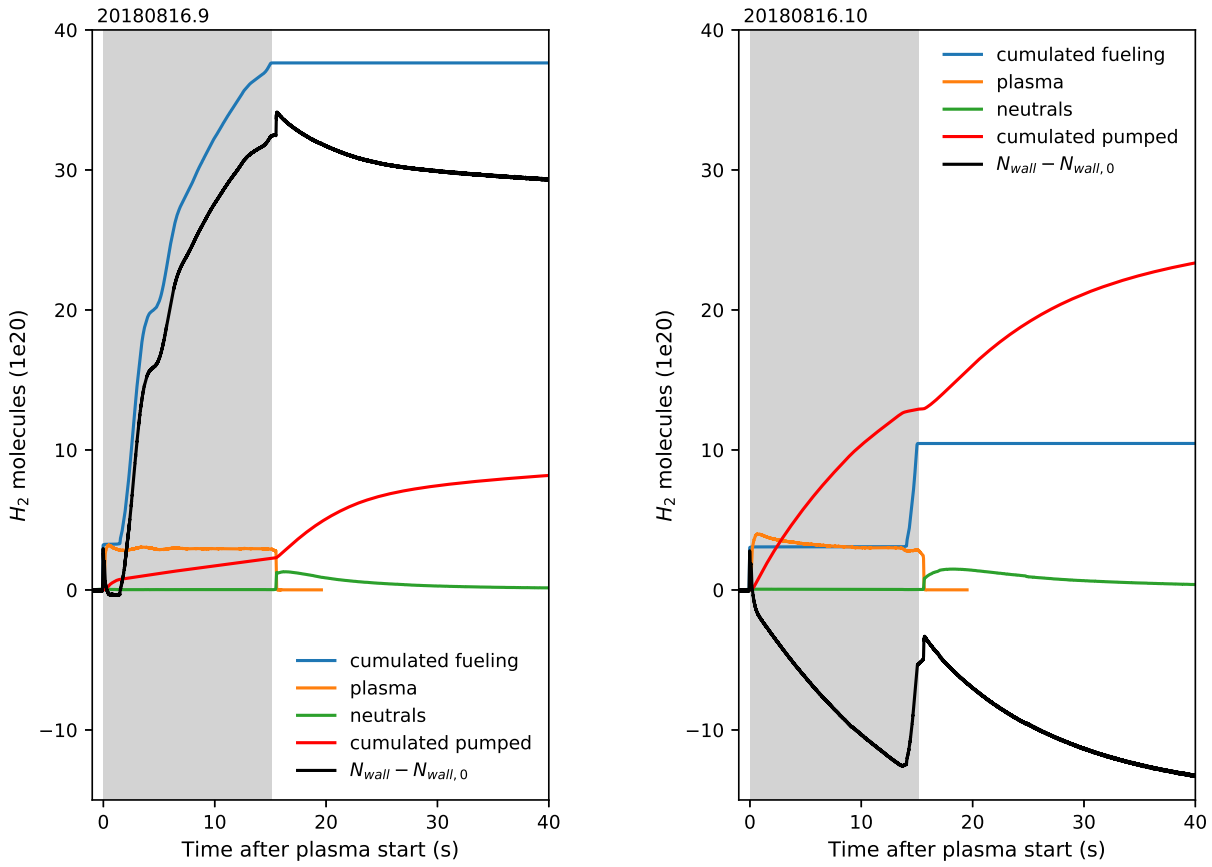

FIG. 6. Comparison of two consecutive plasmas with very similar line-integrated density but low (left) and high (right) heating power and resulting divertor temperature. See figure 5 for plasma parameters. With the poorly heated divertor and heavy fueling, a huge wall reservoir builds up and the following plasma can sustain (apart from a prefill) entirely on gas from the wall. The fueling pulse at the very end of the second plasma is a reaction of the feedback control system to compensate the density loss originating from ECRH power drop and does not indicate wall depletion. Plotting details as in figure 4. (color online)

any fueling to even exceed target density. Figure 5 shows an overview of both programs. The low heating power in the first plasma resulted in low deposited power on the divertor, whose maximum surface temperature stabilized at 450 K. The baffle temperature remained nearly unchanged at 360 K.

The effect on wall behavior is shown in figure 6. Low wall recycling on cold walls leads to a massive retention of gas and required strong fueling in the first experiment. The wall retained $3 \cdot 10^{21}$ additional particles, about ten times the plasma content molecular gas equivalent, after the plasma phase. During the outgassing phase, that reduced by more than a factor of three to $8 \cdot 10^{20}$

during the outgassing phase, still loading the wall with more than double the entire plasma particle molecular equivalent.

On the following attempt with full heating, no external fueling besides the prefill was required. The attaching plasma heated the inertially cooled divertor plates, but left the baffle at nearly the same temperature as before. The heat-up mobilized more particles than needed to sustain plasma density leading to an overshoot. At the same time, high divertor pressures of $1 \cdot 10^{-4}$ mbar allowed efficient exhaust. The fueling pulse towards the end tried to compensate the density decrease due to heating power loss and associated density drop. In total, the program removed about $1.3 \cdot 10^{21}$ molecules from the wall by the end of heating, which is about double of the retained fuel from the previous plasma. Further outgassing removes more than that again, leading to a release of $3.7 \cdot 10^{21}$ molecules from the wall.

This demonstrates the strong influence of the wall history over multiple pulses, where fuel can be retained and released very dynamically.

V. LONG TERM RESERVOIR

One of the highlights of the first divertor campaign of W7-X was the demonstration of a long stable plasma reaching a duration of 100 s at 2 MW of ECRH power and a line-integrated density of $5 \cdot 10^{19}\,\mathrm{m}^{-2}$. Due to safety concerns with respect to the inertially cooled divertor, total injected power per experiment was restricted to 200 MJ, resulting in a rather low maximum heating power. The program was conducted in the *high iota* magnetic configuration, where the main plasma-wall-interaction point is located on the high-iota divertor target. That divertor target was only used in 14% of all experiments and did not experience as varied heat loads as the main divertor target. In result, deeper layers of the fine grain graphite were presumably not as well conditioned as other targets, and the long heating phase needed to be prepared by shorter experiments, even though this experiment was conducted towards the end of the campaign after long initial glow-discharge cleaning, multiple boronizations and an extended experiment program improving wall conditions.

The 100 s plasma was prepared by a sequence of three similar plasmas with duration of about 40 s, 60 s and 80 s for operational reasons. The first experiment of the series lasted for 40 s and showed perfectly flat heating and density time traces. In the following longer experiments however, the density started to rise towards the end, indicating the presence of a strong particle source in the plasma vessel. Figure 7 shows the gas balance of all four consecutive programs. The onset of

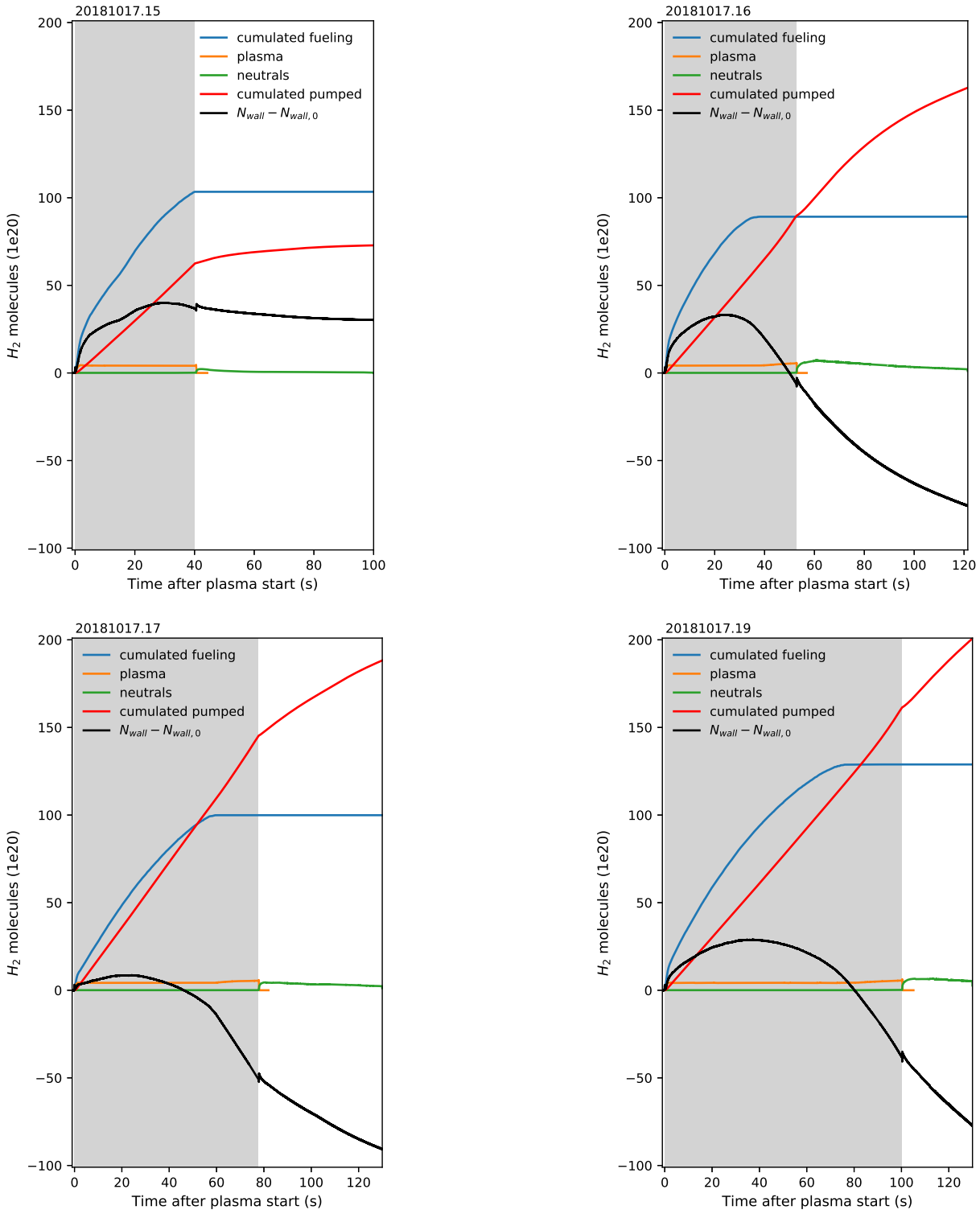

FIG. 7. Gas balance of the four consecutive programs leading up to the 100 s plasma. Number 18 was a failed attempt with no injected power and has no significance for the reported balance and has thus been left out. The net wall reservoir increases at first, turns over and gets negative eventually, about when the external fueling ceases and plasma particle reservoir shows a slight increase as well. This indicates a strong wall source not fully compensated by the exhaust. Plot details as in figure 4. (color online)

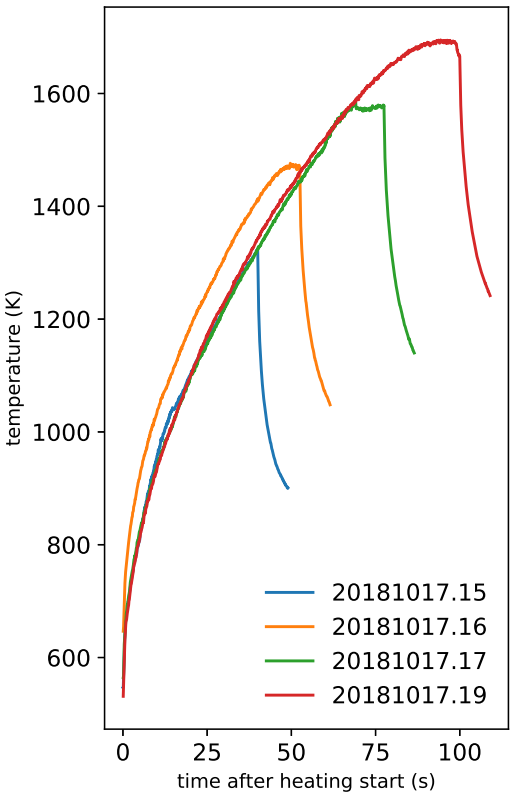

FIG. 8. Divertor tile maximum surface temperature evolution of the same programs as in figure 7. All programs exhibit the same behaviour, the slightly higher temperature in the second program is due to an elevated base temperature. (color online)

the density increases coincides with the end of auxiliary hydrogen gas fueling in density-feedback mode.

In the 40 s and 80 s plasma (20181017.15 and .17) NBI blips were introduced over a 10 s period, which required an opening of the NBI gate valve and resulted in additional particle removal. In the former, the NBI blips were introduced in the beginning, in the latter near the end. The particle input through the blips is minimal and is not considered here, the particle removal is higher but quantitatively unknown due to a lack in diagnostic. This introduces a perturbation on the removed particles, which does not change the overall picture and is thus not taken into account.

The surface temperature evolution of the divertor plates shown in figure 8 exhibits very similar heat-up for all pulses until the termination of plasma heating, plasma decay and subsequent inertial cooling of the divertor plates. A shorter cool-down phase before the second pulse resulting in an elevated base temperature of the divertor graphite tiles explains the moderately higher temperatures in the second pulse (20181017.16), which matches the other pulses in shape.

The inferred wall reservoir in figure 7 exhibits an interesting effect in all programs: after an initial phase of net retention it turns over and reaches net release around the time when the density starts to rise. This is understood as the wall particle source increasing with surface temperature,

leading from initial net wall retention to net wall outgassing as the divertor tile temperature increases. The shift of this transition to later times and higher surface temperatures indicates, that particle reservoirs inside the graphite tiles are increasingly depleted and the outgassing happens only at higher surface temperatures. A plausible explanation is the spread of heat into the full divertor tile and even its holding structure.

A slight increase in the water signal in all RGAs indicates, that water is part of the released gas, presumably from previously unheated divertor parts. Due to the remaining boron layer from boronization, the oxygen is quickly gettered and does not strongly radiate in the plasma edge. The remaining hydrogen fuels the plasma and is measured as additional fueling source, which successively replaces the external gas fueling and leads to an increase in plasma density, when it exceeds the loss channels and the external gas fueling has ceased.

The net wall inventory in the first program is still slightly positive, with $7 \cdot 10^{20}$ retained particles at the end of the outgassing phase, and turns strongly negative for the following programs, reaching a level of about $2 \cdot 10^{22}$ removed molecules per program, of which up to a quarter was removed already during plasma. Overall, the sequence removed more than $7 \cdot 10^{22}$ particles from the wall, which is about 4% of the estimated total reservoir in the carbon divertor.

It is concluded that the 100 s plasma could not be conducted without the preceding steps to condition the divertor, since the strong wall source otherwise would have raised the plasma density beyond the limit that can be sustained with the given heating power. For the upcoming campaigns with a water-cooled divertor, the picture however might change significantly. While the initial conditioning might take longer due to reduced outgassing time after plasma wetting, the heat cannot spread widely through the components and is hopefully efficiently exhausted without mobilizing deep reservoirs in the graphite. Also, the total amount of graphite is reduced in the divertor.

VI. CONCLUSIONS

We have shown a gas balance for W7-X with an inertially cooled graphite divertor in attached scenarios. A wide range of operation regimes exists in varying wall conditions which either fill or deplete the wall with significant amount of hydrogen.

Significant wall heating is key to mobilize retained gas in the carbon structures, while auxiliary fueling on low-heated walls leads to strong fuel absorption. Even in a well-conditioned machine, preparatory plasma experiments were required to prepare long plasma experiments.

scenario	experiment ID	plasma duration	total injected	total removed	net wall	removed/injected
Simple plasma (section III)	20180829.6	4 s	3.23	25.9	−22.7	8.02
short term retention (section IV)	20180816.9	15 s	37.6	30.0	7.60	0.80
	20180816.10	15 s	10.5	47.3	−36.8	4.50
long term retention (section V)	20181017.15	40 s	103	95.9	7.10	0.93
	20181017.16	53 s	89.2	287	−198	3.22
	20181017.17	78 s	99.9	344	−244	3.44
	20181017.19	100 s	129	402	−273	3.12

TABLE II. Overview of total injected and removed particles as well as net wall result, for all discussed experiments. All particle numbers are given as 10^{20} H_2 molecules. Last column shows ratio of injected and removed particle count for easier comparison.

Especially after boronization, the influx of oxygen into the outer plasma could be well controlled even when mobilizing deep reservoirs containing water. Table II shows an overview of all discussed plasma scenarios and their key figures.

A systematic study beyond the shown cases could add to a better understanding of the long-term conditioning effect of plasma operation, which is important with respect to the steady-state target of W7-X in the future.

With a fully water-cooled first wall in future campaigns, equilibrium wall conditions during plasma will be easier to reach and should present a favorable environment for further plasma investigations. Both attached and detached plasmas will be able to reach steady wall conditions, and assessment of wall conditions will hopefully become much easier. Also, the available wall reservoir potentially shrinks, as the bulk material will not heat up as much anymore due to active cooling. The outgassing phase on the other hand will be shortened significantly due to rapid cooling of bulk and surface material, requiring different wall conditioning approach than with an inertially cooled divertor.

ACKNOWLEDGMENTS

This work has been carried out within the framework of the EUROfusion Consortium and has received funding from the Euratom research and training programme 2014-2018 and 2019-2020 under grant agreement No 633053. The views and opinions expressed herein do not necessarily reflect those of the European Commission.

---

[1] T. Loarer, et al., 20th IAEA fusion energy conference proceedings (2005): 36078348.

[2] C. Beidler et al., Fusion Technology 17 (1990): 148.

[3] J. Boscary, et al., Fus. Eng. Des. 86 (2011): 572.

[4] T.S. Pedersen, et al., Physics of Plasmas 24 (2017): 055503.

[5] T.S. Pedersen, et al., PPCF 61.1 (2018): 014035.

[6] S.L. Allen, et al., 23rd IAEA fusion energy conference proceedings (2010): 11.

[7] V. Rohde, et al., Nucl. Fusion 49 (2009): 085031.

[8] V. Rohde, et al., PPCF 51 (2009): 124033.

[9] G. Motojima, et al., J. Nucl. Mat. 463 (2015): 1080.

[10] Y. Nakamura, et al., J. Nucl. Mat. 290-293 (2001): 1040.

[11] M. Oberkofler, et al., J. Nucl. Mat. 438 (2013): S258.

[12] Y. Yu, et al., PPCF 54 (2012): 105006.

[13] T. Loarer, et al., Nucl. Fusion 47 (2007): 1112.

[14] T. Tanabe, et al., J. Nucl. Mat. 313 (2003): 478.

[15] G. Schlisio, et. al., Rev. of Sci. Inst. 90.9 (2019): 093501.

[16] C. P. Dhard, et al., Fus. Eng. Des. 146 (2019): 242.

[17] F. Reimold, et al., Nucl. Fusion 55 (2015): 033004.

[18] A. Drenik, et al., Fus. Eng. Des. 124 (2017): 239.

[19] K.J. Brunner, et al., J. Inst. 13 (2018): 09002.

[20] O.P. Ford, et al., Rev. of Sci. Inst. 91 (2020): 023507.

[21] M. Kubkowska, et al., Fus. Eng. Des. 136 (2018): 58.

[22] W. Biel, et al., Rev. of Sci. Inst. 77 (2006): 10F305.

[23] A. Pavone, et al., J. Inst. 14 (2019): C10003.

[24] U. Wenzel, et al., Rev. Sci. Inst. 90 (2019): 123507.

[25] G. Haas, H.S. Bosch, Volume 51/1 (1998): 39-46.

[26] T. Kremeyer, et al., Rev. Sci. Inst. 91 (2020): 043504.

[27] H. Grote, et al., Journal of Nuclear Materials 313316 (2003): 1298-1303.

[28] Y. Feng, et al., Contr. Plasma Physics 54.4-6 (2014): 426.

[29] J. Schacht, et al., Fus. Eng. Des. 129 (2018): 6.

[30] T. Barbui, et al., J. Inst. 14.07 (2019): C07014.

[31] M. Dibon, et al., Fus. Eng. Des. 98 (2015): 1759-1762.

[32] T. E. Gebhart, et al., Fusion Science and Technology 75.2 (2019): 89-97.

[33] R. Bussiahn, et al., Rev. Sci. Inst. 89 (2018): 10K112.

[34] T. Wegener, et al., Rev. Sci. Inst. 89 (2018): 073505.

[35] P. McNeely, et al., Fus. Eng. Des. Volume 88, Issues 68, (2013): 1034-1037.

[36] T.S. Pedersen, et al., Nucl. Fusion 59 (2019): 096014.

[37] A.P. Zakharol, et al., Journal of Nuclear Materials 241-243 (1997): 52-67.

[38] H. Niemann, et al., Nucl. Fusion 60 (2020): 084003.

[39] E. Denisov, et al., J. Nucl. Mat. 233 (1996): 1218.

[40] H. Atsumi, J. Nucl. Mat. 307 (2002): 1466.

[41] T. Hino, et al., Vacuum 83 (2008): 493.

[42] T. Hino, et al., J. Nuc. Mat. 386 (2009): 736.